



# Qualitative and quantitative changes in detrital reservoir rocks caused by CO<sub>2</sub>–brine–rock interactions during first injection phases (Utrillas sandstones, northern Spain)

E. Berrezueta<sup>1</sup>, B. Ordóñez-Casado<sup>1</sup>, and L. Quintana<sup>1,2</sup>

<sup>1</sup>Instituto Geológico y Minero de España, Oviedo, Spain

<sup>2</sup>Departamento de Geología, Universidad de Oviedo, Oviedo, Spain

Correspondence to: E. Berrezueta (e.berrezueta@igme.es)

Received: 30 June 2015 – Published in Solid Earth Discuss.: 11 August 2015

Revised: 30 November 2015 – Accepted: 2 December 2015 – Published: 15 January 2016

**Abstract.** The aim of this article is to describe and interpret qualitative and quantitative changes at rock matrix scale of lower–upper Cretaceous sandstones exposed to supercritical (SC) CO<sub>2</sub> and brine. The effects of experimental injection of CO<sub>2</sub>-rich brine during the first injection phases were studied at rock matrix scale, in a potential deep sedimentary reservoir in northern Spain (Utrillas unit, at the base of the Cenozoic Duero Basin).

Experimental CO<sub>2</sub>-rich brine was exposed to sandstone in a reactor chamber under realistic conditions of deep saline formations ( $P \approx 7.8$  MPa,  $T \approx 38$  °C and 24 h exposure time). After the experiment, exposed and non-exposed equivalent sample sets were compared with the aim of assessing possible changes due to the effect of the CO<sub>2</sub>-rich brine exposure. Optical microscopy (OpM) and scanning electron microscopy (SEM) aided by optical image analysis (OIA) were used to compare the rock samples and get qualitative and quantitative information about mineralogy, texture and pore network distribution. Complementary chemical analyses were performed to refine the mineralogical information and to obtain whole rock geochemical data. Brine composition was also analyzed before and after the experiment.

The petrographic study of contiguous sandstone samples (more external area of sample blocks) before and after CO<sub>2</sub>-rich brine injection indicates an evolution of the pore network (porosity increase  $\approx 2$  %). It is probable that these measured pore changes could be due to intergranular quartz matrix detachment and partial removal from the rock sample, considering them as the early features produced by the CO<sub>2</sub>-rich brine. Nevertheless, the whole rock and brine chemical anal-

yses after interaction with CO<sub>2</sub>-rich brine do not present important changes in the mineralogical and chemical configuration of the rock with respect to initial conditions, ruling out relevant precipitation or dissolution at these early stages to rock-block scale. These results, simulating the CO<sub>2</sub> injection near the injection well during the first phases (24 h) indicate that, in this environment where CO<sub>2</sub> enriches the brine, the mixture principally generates local mineralogical/textural re-adjustments on the external area of the samples studied.

The application of OpM, SEM and optical image analysis have allowed an exhaustive characterization of the sandstones studied. The procedure followed, the porosity characterization and the chemical analysis allowed a preliminary approximation of the CO<sub>2</sub>–brine–rock interactions and could be applied to similar experimental injection tests.

## 1 Introduction and objectives

The capture and geological sequestration of CO<sub>2</sub> is one of the technological options currently contemplated to reduce emissions of greenhouse gases into the atmosphere. Deep geological storage in porous rock formations is considered the most appropriate strategy for CO<sub>2</sub> sequestration (Bachu, 2000; Izgec et al., 2008; Benson and Cole, 2008; Gaus, 2010) and injectivity is a key technical and economic issue for carbon capture and storage (CCS) projects (Bacci et al., 2011). The viability of the CO<sub>2</sub> injection depends mainly on the porosity and permeability of reservoir rocks. CO<sub>2</sub> interaction with the host rock, such as dissolution or precipitation

of minerals is also important (e.g. Ross et al., 1982; Sayegh et al., 1990; Saeedi et al., 2011), as well as mineral trapping (Kaszuba et al., 2003; Rosenbauer et al., 2005; Liu et al., 2013). Dissolution of supercritical (SC) CO<sub>2</sub> into brine will control the rate of dissolution and precipitation of minerals constituting the porous rock. Volume changes of the solid phase will modify the pore structure, affecting both porosity and permeability of the porous media (André et al., 2007).

CO<sub>2</sub>–water–rock interaction experiments represent a useful method to understand and explore the mechanisms and processes of geological storage (Ketzer et al., 2009) and to design safe underground CO<sub>2</sub> storage operations. Bertier et al. (2006) built an experimental setup to evaluate the effect of CO<sub>2</sub>–water–rock interactions in three sandstone aquifers concluding that “CO<sub>2</sub>–water–rock interactions might significantly influence geological sequestration of CO<sub>2</sub>”. Most of the experimental and theoretical studies are designed to simulate the injection of CO<sub>2</sub>, mixed with brine, into rocks at *P-T* conditions of deep storage environments. The result of many of these experiments was an increase in the porosity/permeability of the reservoir rock caused by partial dissolution of the carbonate components (mainly calcite) (Perkins and Gunter, 1995; Svec and Grigg, 2001; Rochelle et al., 2004; Egermann et al., 2005; Izgec et al., 2005; Gunter et al., 2004; Luquot and Gouze, 2009; Desbois et al., 2011). However, another set of experiments has shown porosity decreases due to the initial dissolution of carbonates followed by secondary precipitation/mineralization (Kaszuba et al., 2003, 2005; Cailly et al., 2005; Mito et al., 2008; Sterpenich et al., 2009; Luquot and Gouze, 2009). André et al. (2007) presented numerical modelling of chemical fluid–rock interactions at the SC-CO<sub>2</sub>-liquid interface during CO<sub>2</sub> injection into a carbonate reservoir (Paris Basin, France). In this case, two CO<sub>2</sub> injection scenarios were evaluated: CO<sub>2</sub>-saturated water injection and pure supercritical CO<sub>2</sub> injection. In these two scenarios, different geochemical processes occurred as the distance from the injection well increased (in the first scenario there was a porosity increase of up to 90%; while, in the second scenario porosity increased about 6% in most of the reservoir and it decreased in the vicinity of the injection point). Besides, different regions were identified depending on the saturation ranges of liquid and gas phases, associated geochemical conditions and porosity variations during the injection and according to the distance from the injection well (Fig. 1a).

Other investigations focus on the CO<sub>2</sub> injection into potential reservoir rock formations under dry conditions (Kaszuba et al., 2003; Vickerd et al., 2006; Berrezueta et al., 2013). The injection environment is mainly envisaged as injecting CO<sub>2</sub> mixed with brine into sandstones. However, in near-well conditions, the supercritical CO<sub>2</sub> laterally displaces the brine and occupies the pore space of the rocks, in either dry or near-dry conditions (André et al., 2007; Burton et al., 2008; Luquot and Gouze, 2009; Gaus, 2010). Therefore, dry CO<sub>2</sub> interaction with the storage rock is a realistic scenario that

takes place during the initial injection stages. Some theoretical studies (Gaus et al., 2008, 2010) and experimental results (Sterpenich et al., 2009) on dry CO<sub>2</sub>–rock interactions indicate the absence of reactions and consequently negligible textural-mineralogical changes. This is explained by the lack of H<sub>2</sub>O in the system that prevents dissolution/precipitation and any kind of chemical reactions. However, experimental studies on dry-CO<sub>2</sub> injection into undersaturated sandstones with high clay matrix content (Berrezueta et al., 2013) concluded in an increase of rock porosity, causing a textural change. This was explained by detachment and partial removal of the intergranular clay matrix from the sandstone samples due to supercritical CO<sub>2</sub> input/release dragging and changes in electrical-polarity forces.

Our research is focussed on experimental injection of supercritical CO<sub>2</sub> into the selected rocks (sandstones saturated by and covered with brine), similarly to previous works, e.g. Tarkowski and Wdowin (2011), Fischer et al. (2013), Wdowin et al. (2014a, b) and Tarkowski et al. (2015). We chose the Utrillas sandstones for the present study due to their importance as potential CO<sub>2</sub> reservoirs in Spain. The lithological characteristics of the Utrillas sandstones and the structural features of the area offer favourable conditions for the study of CO<sub>2</sub> storage (García Lobón et al., 2010; Martínez et al., 2013).

The selected *P-T* conditions and runtimes of our experiments aim to reproduce the reservoir rock dry–wet environment, adjacent to a theoretical injection borehole, (Fig. 1a and b), specifically, at the interface between the supercritical CO<sub>2</sub> bubble and the aqueous solution. This interface acts as an exchange zone where CO<sub>2</sub> diffuses constantly (e.g. Zone 4 defined by André et al., 2007). The experimental *P-T* conditions were selected to guarantee that the CO<sub>2</sub> was over its supercritical point (Holloway, 1997; Bachu, 2000; Lake 1989; Span and Wagner, 1996).

Furthermore, the textural-mineralogical and petrophysical changes in the rock samples are studied before and after the experimental injection of supercritical CO<sub>2</sub> for a short period of time (24 h). Special care was put into the development of a simplified model to explain the observed changes. Optical image analysis (OIA) techniques were used to monitor these changes.

## 2 Samples: geological setting

The studied samples belong to the unit commonly known as Utrillas sandstones and locally defined as the Voznuevo Formation (Evers, 1967) of upper Albian–lower Cenomanian age (lower–upper Cretaceous transition). The sampling took place in northern Spain, at the boundary between the Alpine Cantabrian Mountains and the Cenozoic Duero Basin (Fig. 2a). The Utrillas sandstones belong to a 1100 m thick Cretaceous sequence and crop out near Boñar village in the northern León province. This Cretaceous sequence lays

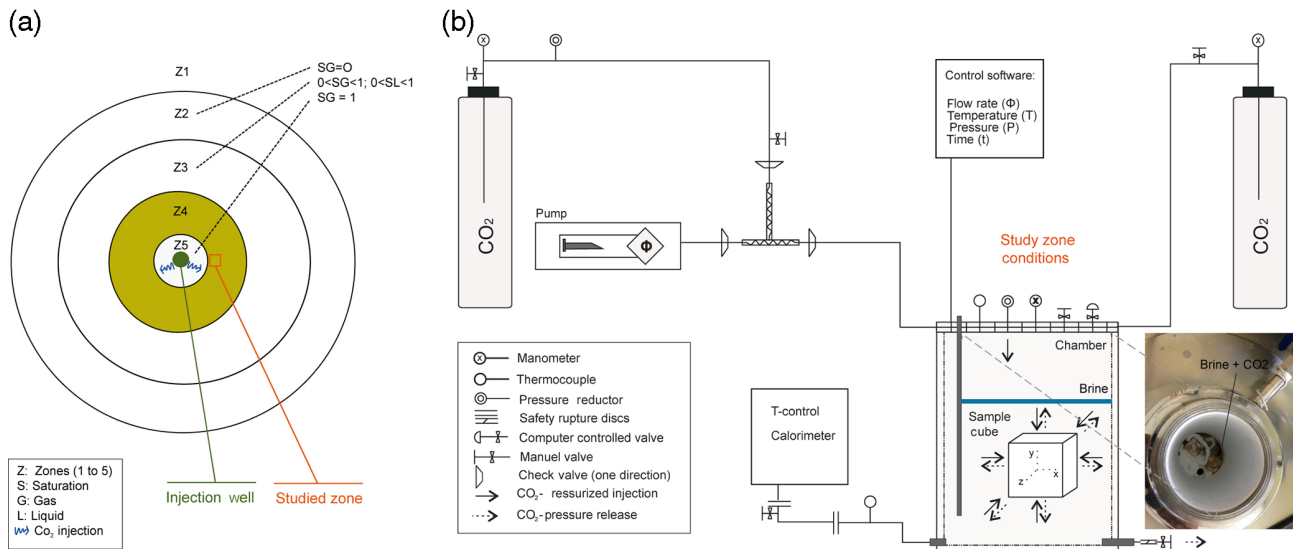


**Figure 1.** (a) Conceptual diagram of the reactive zones (Z1, Z2, Z3, Z4 and Z5) around the injection well according to André et al. (2007) and Gaus et al. (2008). Zone 1: zone not affected by  $\text{CO}_2$  injection; Zone 2: acidified zone with dissolution and precipitation of minerals. Zone 3: Dissolution and precipitation of minerals (e.g. calcite and dolomite) and highly buffered pH. Zone 4: Highly saline water and salt precipitation (e.g.  $\text{NaCl}$  and  $\text{Mg}_2\text{SO}_4$ ). Zone 5: Dehydration reactions in open systems. (b) Layout of the experimental setup. Reactor system used for the pressurized  $\text{CO}_2$  injection (modified from Berrezueta et al., 2013).

unconformably on the Paleozoic basement of the Variscan Cantabrian Zone. On top of the Cretaceous sequence, a succession of almost 2500 m thick Cenozoic materials was deposited in the Duero Basin (Fig. 2d). The Cretaceous sequence has been divided into three parts (Manjón Rubio et al., 1982a): (1) a lower detrital part, which corresponds to the Utrillas sandstones, of continental origin; (2) an intermediate or transitional part of Turonian-Santonian age; and (3) an upper carbonate part with limestones and marls of Santonian-Campanian age and marine origin (Fig. 2c). This Cretaceous sequence was deposited in a post-rift stage, at the end of the Cretaceous extensional phase that affected northern Spain and produced the opening of the Bay of Biscay (e.g. Gallastegui, 2000).

The Utrillas sandstones, in the study area, are composed of detrital, poorly consolidated or unconsolidated whitish materials ranging from sandstone to conglomerate, with a maximum size of pebbles of 6 cm. The succession is fining upwards with dominating conglomerates at the base and progressively increasing sandstone ratio. The pebbles and grains are mainly of quartzite origin and of subrounded to subangular form, with a sandy and kaolinitic matrix. Argillaceous levels, palaeochannels and cross-stratification are frequent and lignites appear locally. This succession was formed in a fluvial braided environment and with a source area composed of acid, mainly granitic and metamorphic, rocks. The transformation from feldspar to kaolin occurred after the deposition and was the result of meteorization processes (Manjón Rubio et al., 1982a).

The fluvial environment, in which the Utrillas sandstones were formed, represents the proximal part of the upper Cretaceous north Iberian palaeomargin. Towards the north, this fluvial facies changed into deltaic facies, then talus facies and, finally, deep basin turbiditic facies (Olivé Davó et al., 1989). This palaeomargin was deformed during the collision between Iberia and Eurasia in Cenozoic times. This compressional event produced the uplift of the Cantabrian Mountains in northern Spain and the development of the Duero foreland basin in the frontal part of the range (Alonso et al., 1996). The structure of the sampling area is relatively simple and is characterized by a great monocline (Fig. 2d), the formation of which has been related with a south-directed basement thrust inclined to the north (Alonso et al., 1996). In detail the structure is more complex because the inclined limb of the monocline is disrupted by an important fault, known as the Sabero Fault (Sabero-Gordón line of Rupke, 1965), that produces the duplication of the Cretaceous sequence (Fig. 2b and d).

The Utrillas sandstone was sampled in three places of the complex inclined limb of the monocline, in the area of Devesa de Boñar, performing a thorough study of the structure of these target rocks and their seals (Fig. 2b, d and e). The sampling areas “Devesa 1” and “Devesa 2” are located south of the Sabero Fault, in an outcrop of Cretaceous succession dipping  $80^\circ$  towards the south. The sampling area “Devesa 3” is located north of the Sabero Fault in an outcrop dipping  $45^\circ$  also southwards (Fig. 2b and d). For this study, we chose the more consolidated sandstones (3 samples), located in “Devesa 1”, to guarantee the effectiveness of the analysis. The

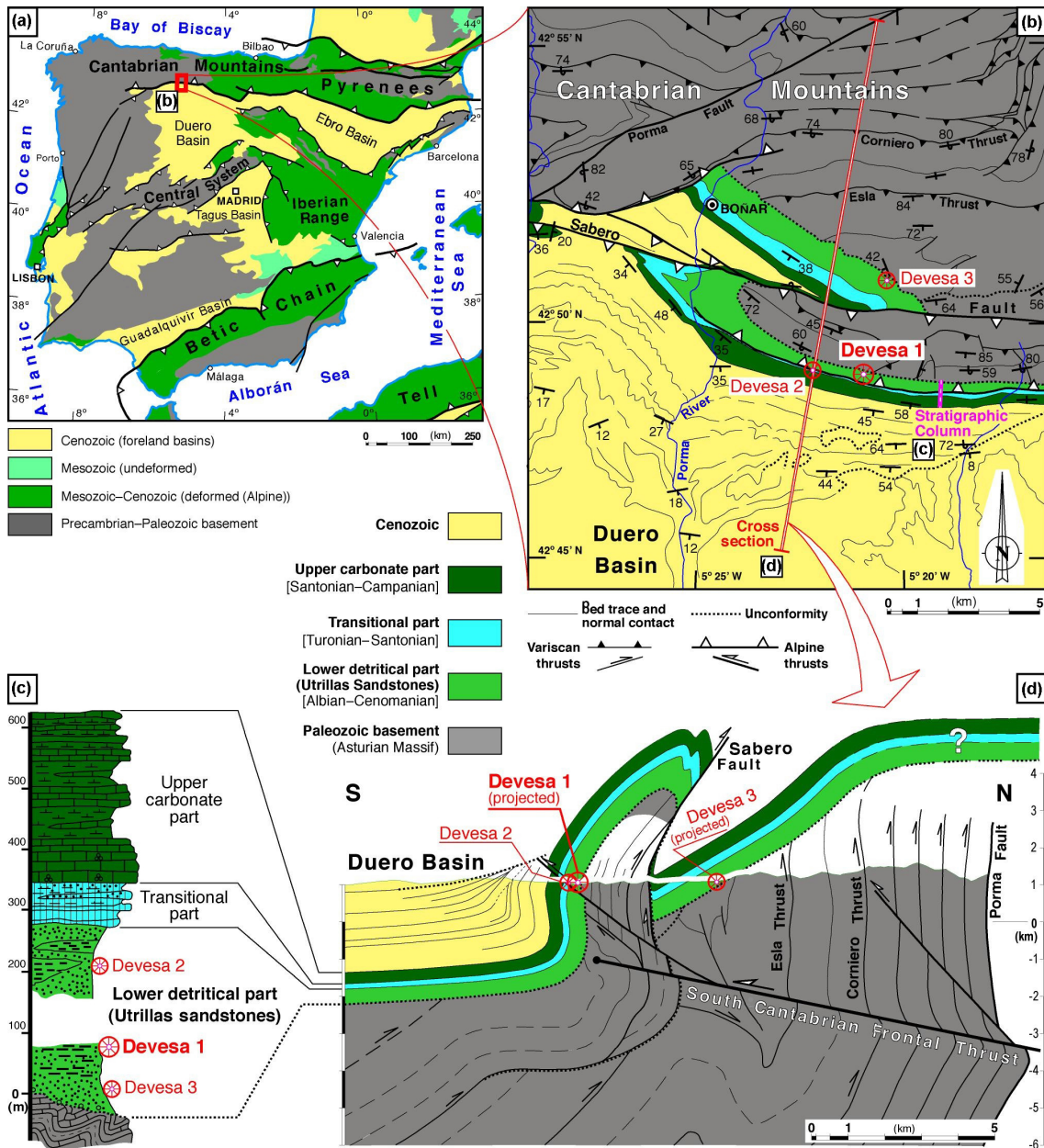


**Figure 2.** (a) Location of the studied area in northern Spain; modified from Quintana et al. (2015) (b) Geological map and location of the sampling areas modified from Lobato et al. (1985), Manjón Rubio et al. (1982b) and Alonso et al. (1996). (c) Stratigraphic column of the Cretaceous succession of the studied area. Location in (b). Manjón Rubio et al. (1982b). (d) Geological cross-section along the sampling areas: boundary between the Cantabrian Mountains and the Duero Basin. The geometry of the South Cantabrian Frontal Thrust and of the Cenozoic materials of the Duero Basin taken from Alonso et al. (1996). Location in (b).

unconsolidated sandstones of Devesa 2 and 3 were discarded for the study. The samples were divided into adjoining and numbered sets of blocks. Each couple of adjoining blocks was used for the experimental test and for the studies before and after CO<sub>2</sub> injection.

### 3 Methodology and experimental procedure

#### 3.1 Experimental setup and procedure

The experimental setup employed in this experiment (Fig. 1b) is based on similar systems described by Luquot and Gouze (2009), Tarkowski and Wdowin (2011), Luquot et al. (2012), Berrezueta et al. (2013) and Wdowin et al. (2014a,

b). However, some modifications were made due to the distinct characteristics of the target rock system. Sample material (rock-type and representative sample size), geological environment (pressure, temperature and salinity) and technical equipment (materials for camera, software, pumps etc.) were all considered for the final arrangement of the experimental device and run conditions. The experiment consists of the exposure of sandstones to CO<sub>2</sub>-rich brine in a reactor with pressure and temperature control. *P/T* conditions (7.8 MPa and 38 °C, respectively) were selected to surpass the CO<sub>2</sub> supercritical point (Lake, 1989; Span and Wagner, 1996) and to simulate basic conditions of injection and storage of CO<sub>2</sub> (Holloway, 1997; Bachu, 2000). These conditions are representative of a depth of approx. 800 m. The selected exposure time (24 h) is meant to model the first stage of injection. The brine used in the experiments is natural brine from a borehole from a saline aquifer.

The system (Fig. 1b) has two CO<sub>2</sub> cylinders (standard industrial CO<sub>2</sub> at 4.5 MPa) that are linked to the other elements of the system by steel connectors (diameter: 5 mm). The second CO<sub>2</sub> cylinder is connected to a piston pump that operates with a flow of 0.01 g s<sup>-1</sup>. In case of gas leakage in the chamber during the experiment, this pump maintains the experimental pressure (7.8 MPa). The piston pump needs a CO<sub>2</sub> initial pressure of 1 MPa in order to inject CO<sub>2</sub> into the Hastelloy steel chamber (3 dm<sup>3</sup>), thereby, the pressure between the piston pump and the second CO<sub>2</sub> cylinder has to be decreased by a pressure manometer from 4.5 to 1 MPa. The inside of the chamber is coated with polytetrafluoroethylene (PTFE) to protect the material against corrosion. At the bottom of the chamber, a calorimeter controls the internal temperature. The calorimeter and the pump are linked to the chamber with pressure and temperature sensors and are connected to a computer.

The experiments began with the saturation of rock samples (six cubes of 27 cm<sup>3</sup> of sandstone sample) with natural brine by three cycles during 72 h. A total of 0.3 dm<sup>3</sup> of this brine was extracted and analyzed before CO<sub>2</sub>-rich brine exposure occurs. Then, the rock samples (six cubes of 27 cm<sup>3</sup> of sandstone sample) were introduced into the chamber and fully immersed in the rest of brine (0.3 dm<sup>3</sup>) and at the end of the experiments analyzed and noted “after CO<sub>2</sub>-rich brine”. The experimental runs comprised: (a) a pressurized CO<sub>2</sub> injection (3 h, from ambient conditions to supercritical conditions); (b) a pressurized stabilization (24 h, no CO<sub>2</sub> flow inside the chamber) and c) CO<sub>2</sub> pressure release (3 h, from supercritical conditions to ambient conditions). In general, the presence of non-dissolved SC CO<sub>2</sub> in the brine was not in contact with the rock. This occupied the top of the test chamber. Sample + brine + CO<sub>2</sub> were up to supercritical conditions for 24 h. Sample + brine + CO<sub>2</sub> were 6 h in conditions below 38 °C and 7.8 MPa.

The CO<sub>2</sub> injection was performed using a constrained hyperbaric chamber-reactor where the dry CO<sub>2</sub> was pumped at pressures and temperatures of 7.8 MPa and 38 °C, respec-

tively. The times of filling and emptying the chamber with supercritical CO<sub>2</sub> were the same (3 h), following the chamber’s manufacturer recommendations. This is the time required to reach the target pressure and temperature values, from the initial ambient conditions. The same time was used to get back to the ambient conditions at the end of the experimental test. The applied software, HEL 5.1, allows the remote control of the system (experimental conditions) through the development of specific macros (pressure, temperature, time) in real time. All the experimental runs were carried out in the laboratories of the Geological Survey of Spain (IGME) in Tres Cantos, Madrid.

### 3.2 Methodology of study

The aim of the study was to quantify the possible textural and porosity changes due to experimental CO<sub>2</sub> injection. We began with a detailed petrographic study using optical microscopy (OpM) to identify the major mineral and textural features. The characterization was performed in neighbouring areas of the blocks by OpM (30 μm thin sections) and scanning electron microscopy (SEM, rock samples). Although the thin sections and SEM samples do not exactly correspond to the same sample surface, they are located very close (a few mm) in the original source sample. The aim of the detailed OpM study and quantification of mineralogical and textural variability was to verify that any changes observed in the experiments were due to the effects of CO<sub>2</sub> effect and not to possible original heterogeneity. Furthermore, chemical analysis of the brine and whole rock before and after SC CO<sub>2</sub> injection were performed, as well as microscopic studies of the residue that remained in the reactor chamber after the experiment.

Simultaneously, a detailed study of the configuration of porous system was conducted by combining observation by scanning electron microscopy with backscattered electrons (SEM) and optical image analysis (OIA). This method allows the study of pore size distribution and other porosity parameters (shape, specific surface of pore etc.). Later, the same procedure was followed for the study of the SC CO<sub>2</sub> exposed rocks. The OIA technique makes it possible to identify, characterize and quantify mineral elements in images captured digitally (Fig. 3) before and after SC CO<sub>2</sub>-brine exposure. The general procedure for the automated image analysis was developed, adapting the procedures and algorithms described by Berrezueta et al. (2015), in order to quantify the textural and porosity changes (area, roughness of minerals/pore boundaries, fractal dimension, roundness of minerals/pores and porosity) provoked by experimental CO<sub>2</sub> injection. Assessment of pore-network distribution by optical transmitted light studies of thin sections requires distinction between mineral and pore networks according to their optical characteristics. The segmentation of the porous system was made by regions, applying the “thresholding” segmentation method (based on threshold values to turn a raw image into

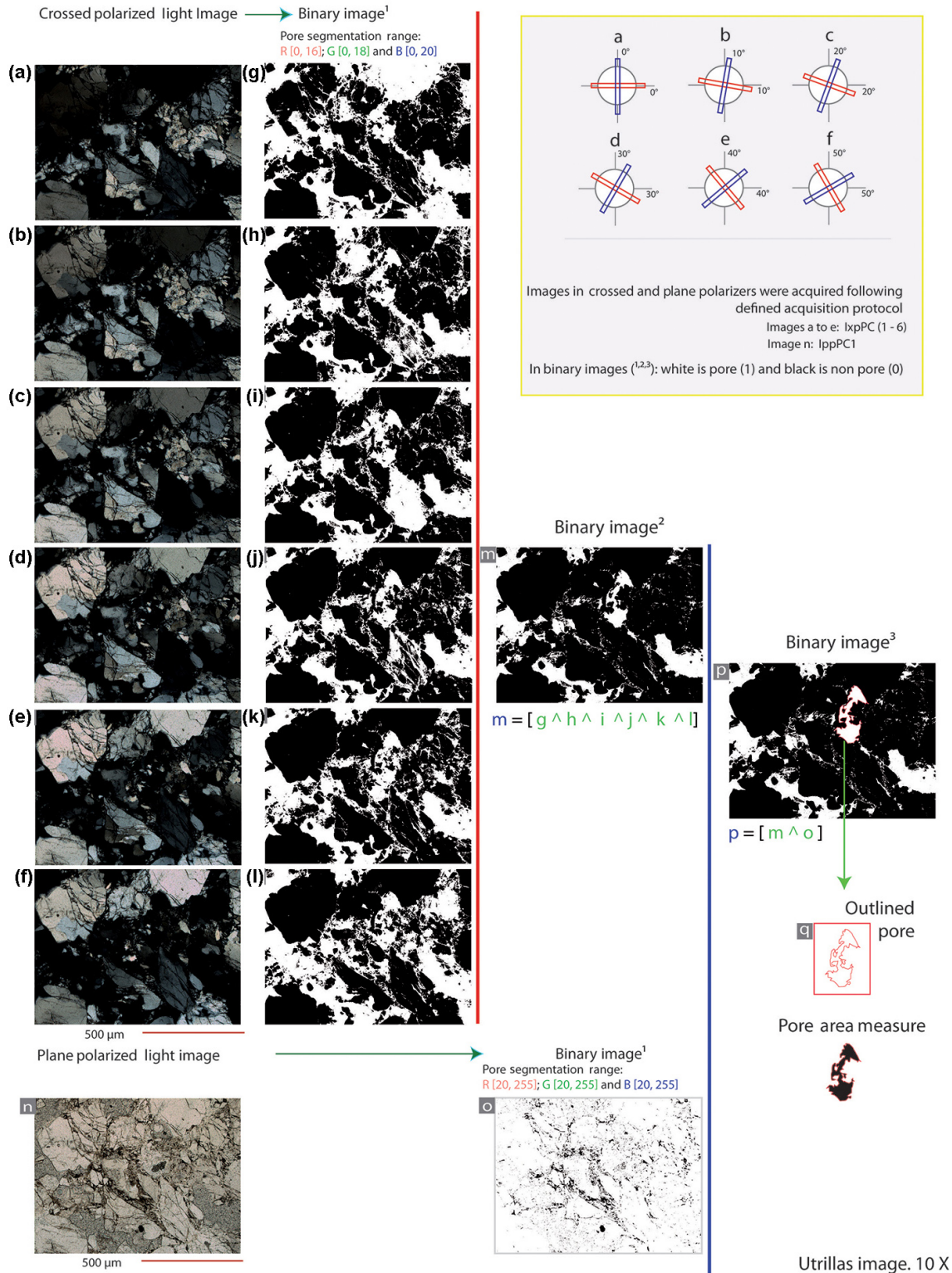


**Figure 3.** Schematic representation of the sequence of pore segmentation and pore area quantification performed on digital images (modified from Berrezueta et al., 2015) of the studied Utrillas sandstone. (a–f) Images under cross polarized light conditions. (g–l) Binary images<sup>1</sup> obtained using pore segmentation ranges: R(0–16); G(0–18) and B(0–20). m) Binary image<sup>2</sup> obtained by the interception of binary images<sup>1</sup> (g–l). (n) Image under plane polarized light conditions. (o) Binary image<sup>1</sup> obtained using pore segmentation ranges: R(20–255); G(20–255) and B(20–255). (p) Binary image<sup>3</sup> obtained by the interception of binary images (m) and (o). (q) Pore outlined image.

a binary one, the pixels being partitioned according to their intensity value). In this way, we can quantify the evolution of small changes in the configuration of the pore network. This work was carried out in the Oviedo IGME laboratory using a Leica DM 6000 polarization microscope with Image Pro Plus-7.0 software and a ProgRes digital camera for pore network study by OIA. SEM studies were performed using a Hitachi TM3000 microscope with X-ray microanalysis equipment.

Additionally, rock samples were analyzed by X-ray fluorescence (XRF) and X-ray diffraction (XRD), and brine composition was determined by several methods (ion chromatography, ICP-OES, pH, conductivity measurements). The studies were developed in the facilities of IGME laboratory-Tres Cantos and Oviedo University. Laboratory and elements analyzed were limited/conditioned to techniques available.

## 4 Results

### 4.1 Mineralogical and petrographic characterization and OIA pore-network quantification

#### 4.1.1 Samples before SC CO<sub>2</sub> injection

The studied rock is a medium to very coarse-grained sandstone (grain size from 90–1600  $\mu\text{m}$ , with a mode of 250  $\mu\text{m}$ ) with areas of fine to medium grain sizes, showing no orientation and slightly to highly variable porous structure. The pores that are 80–500  $\mu\text{m}$  (up to 1400  $\mu\text{m}$ ) in size constitute up to 8–15 % of the rock volume, although there are special areas with porosity up to 20 %. The grains range from moderately to poorly sorted. There are zones with a slight anisotropy defined by the presence of matrix rich bands. The grain skeleton (Fig. 4a, c and e) consists of quartz (>95 %), very minor potassium feldspars (orthoclase) and a small amount of micas (muscovite and chlorite). Accessory minerals (a total of 1–5 %) are opaque minerals, such as iron oxides and hydroxides (hematite and limonite), in the form of aggregates of 40–100  $\mu\text{m}$  in size, dispersed in the matrix or as cement. Other accessory minerals are brown and green tourmalines and zircon. The rock is composed mainly of grain skeleton supported with a small proportion of matrix (<5 %) composed mostly of quartz and minor phyllosilicates of the mica and clay groups (muscovite and/or illite and/or kaolinite) and opaque minerals. Locally, cement is present as a film that coats iron oxides and syntaxial quartz. According to the Folk (1974) and Pettijohn et al. (1987) classification, it is a quartz-arenite (>95 % of quartz). Some areas have higher matrix concentration (>15 %) classified as fine-medium grained quartz-greywacke. The quartz grains are mostly monocrystalline with important size variability. The grains have angular to subangular shapes, from high to low sphericity and with sizes ranging from 90 to 1400  $\mu\text{m}$ . Moreover very rounded grains of polycrystalline quartz (fairly

minor amount) appear sometimes with a Fe oxide coating. They are of significant size (900–1900  $\mu\text{m}$ ). Grains with internal crystals of >30  $\mu\text{m}$  size are the most common. On the other hand, there are some polycrystalline quartz grains with elongated shapes and large dimensions up to 2800  $\mu\text{m}$ . Sometimes the internal crystalline units of the polycrystalline quartz grains show preferred orientations (meta-quartzite origin). The internal units can be of sizes <30  $\mu\text{m}$  (chert) or up to 180–240  $\mu\text{m}$ . The orthoclase feldspars are very scarce, have rounded edges with sizes up to 1400  $\mu\text{m}$  and show a significant degree of alteration to iron oxides, phyllosilicates (illite and/or kaolinite) and chlorite.

The porous system reaches estimated visual proportions of 8–15 %. Adapting Choquette and Pray (1970) and Lucia (1999) porosity nomenclatures for carbonates, various pore types were identified. “Vuggy” pore type, corresponding to highly spherical and rounded pores with sizes around 50–90  $\mu\text{m}$  are common. “Intercrystalline”-type pores were also observed. These are irregularly shaped around skeletal grains with very rounded edges, possibly a product of matrix solution. They present elongated shapes and sizes ranging from 140–220  $\mu\text{m}$  up to 300  $\mu\text{m}$ . There are also incipient “cavernous”-type pores, with elongated shapes, of sizes of ca. 80–170, even 550  $\mu\text{m}$ . In addition, there are “fracture”-type pores. The sizes of these pores generally reach 80–200  $\mu\text{m}$  but there are some larger elongated caverns (ca. 1400  $\mu\text{m}$ ). “Protected” porosity below some quartz grains (500  $\mu\text{m}$ ) was also observed. The mineralogical and pore-network distribution has been corroborated by SEM observation (Fig. 5a, c and e).

The pore network quantification by OIA (Table 1) was carried out in three thin sections with images acquired with a magnification of 10x. The porosity percentage estimated by this method ranges from 6.49 to 18.18 % with an average of  $11.41 \pm 0.14$  %. The maximum and minimum area of pore was 172 100 and 9.2  $\mu\text{m}^2$ , respectively. The average pore area size was 168  $\mu\text{m}^2$ . Curves of relative and absolute distribution of number of pores vs. pore area ranges and diagrams of weighted area related to pore area classes are presented in Figs. 6a and c for the samples before SC CO<sub>2</sub> injection.

#### 4.1.2 Samples after SC CO<sub>2</sub> injection

The studied rock is a medium to very coarse grained, poorly sorted sandstone (particle size from 300–1800  $\mu\text{m}$ ). It is slightly to highly porous with a porosity of 12–18 % of the rock volume and with pore size up to 2.5 mm. The grains vary spherically from high to low and from subrounded to rounded shapes and it is noteworthy that the quartz grains have a high degree of fracturing. The rock has scarce anisotropy, primarily defined by a band of higher matrix concentration and opaque minerals (Fe oxides). The skeleton (Fig. 4b, d and f) consists mostly of quartz grains (>95 %), scarce potassium feldspars (orthoclase) and small amounts of mica (muscovite). Quartz grains show high degree of fracturing and

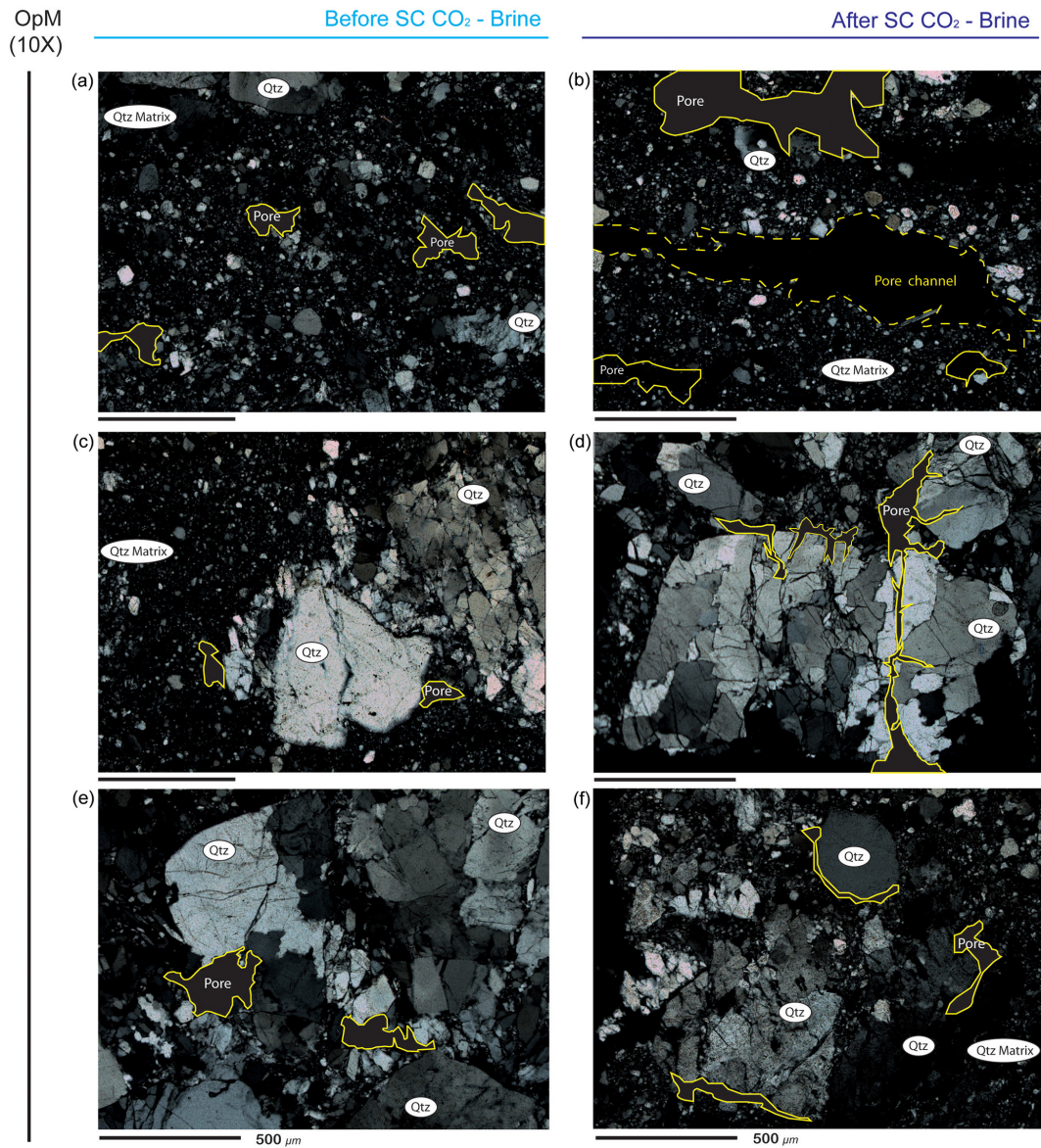


**Figure 4.** Textural and mineralogical characterization of the Utrillas sandstones. Optical microscopy images obtained under cross-polarized light conditions acquired using objective lens of 10 $\times$ . Left images (**a**, **c** and **e**) correspond to samples before SC CO<sub>2</sub> injection; showing the main textural and mineralogical features corresponding to quartz grains and sandy matrix and inter-crystalline pores within the matrix or in the vicinity of skeletal quartz grains. Right images **b**, **d** and **f**) correspond to samples after SC CO<sub>2</sub> injection; showing no changes in the mineralogical features and a pore network characterized by the presence of channels, caverns and pores within large quartz grains.

are primarily monocrystalline with high or low sphericity and rounded edges. Their sizes vary from 300 to 1800  $\mu\text{m}$ . Sometimes they are of low sphericity with rounded edges or subangular shapes, with sizes ranging from 240 to 1000  $\mu\text{m}$ , even up to 2.4 mm. On the other hand, polycrystalline quartz is present with internal crystal units < 30  $\mu\text{m}$ , with elongated shapes, rounded edges and grain sizes between 700 and 1400  $\mu\text{m}$ . Other polycrystalline quartz grains are rounded with sizes up to 1000–2400  $\mu\text{m}$  with internal structural units > 30  $\mu\text{m}$ . Orthoclase feldspars are very rounded and quite spherical, with sizes up to 2.4 mm. They sometimes show

alteration containing Fe oxides and phyllosilicates (possibly illite and /or kaolinite). Accessory minerals are opaque minerals (iron oxides associated to iron hydroxides). These opaque minerals appear in the form of large grains surrounding the skeleton grains or as smaller crystals scattered in the sandy-clay matrix or oriented at the edges of matrix rich bands. Other accessory minerals are tourmaline and zircon. The matrix (< 15 %) is composed mainly of quartz and a small amount of phyllosilicates (possibly illite and/ or kaolinite and/or smectite) and iron oxides. Opaque minerals are Fe oxides and hydroxides (hematite and limonite) that are

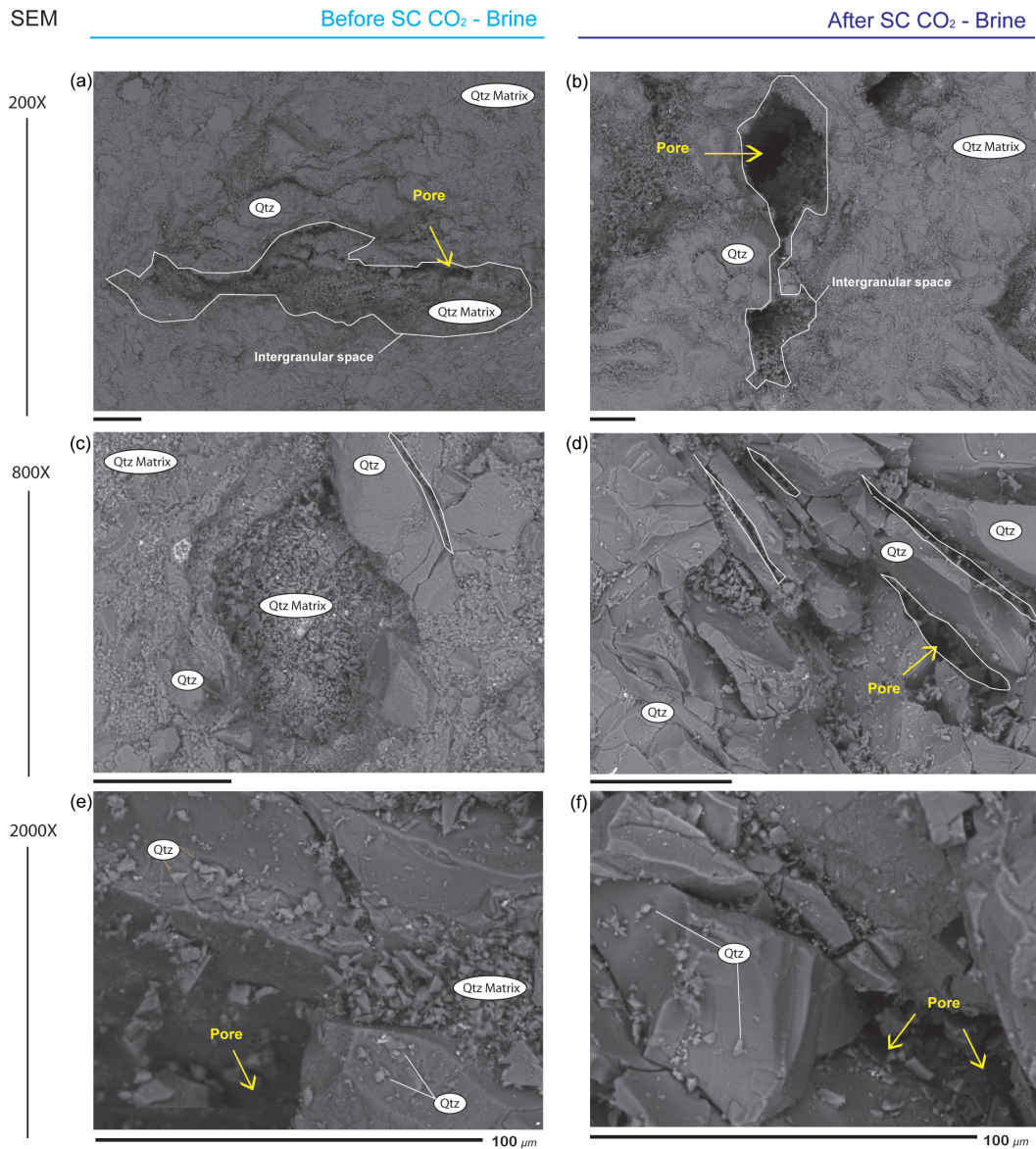


**Figure 5.** Secondary electron SEM micrographs of the Utrillas sandstones. Left images (**a**, **c** and **e**) correspond to samples before SC CO<sub>2</sub> injection. Right images (**b**, **d** and **f**) correspond to samples after SC CO<sub>2</sub> injection. (**a**) Intergranular space filled with minerals; (**b**) intergranular spaces constituted by cavern pores interconnected by micro-channels with pore spaces sometimes filled with minerals; (**c**) intercrystalline space; (**d**) high degree of fracturation of quartz grains; (**e**) the edges of quartz grains in the starting material (before CO<sub>2</sub>-brine exposure) contain angular pits; (**f**) pits in quartz from the experiment are less numerous and distinctly rounded and enlarged.

often associated with phyllosilicates (kaolinite and/or illite and/or smectite) and mica (possibly muscovite). Based on the modal content of quartz, feldspars, lithoclasts and matrix content the rock is classified as quartz arenite and some areas with higher matrix content (ca. 15 %) as medium-grained quartz wacke (Folk, 1974; Pettijohn et al., 1987).

The identified porosity is more abundant than in the samples before CO<sub>2</sub> injection. The estimated visual percentage ranges from 12 to 18 %. Adapting Choquette and Pray (1970) and Lucía (1999) nomenclatures, there are various pore types present in the rock. Intercrystalline pores between quartz

grains with variable sizes (90–240 μm) were observed. The presence of pores that are arranged in micro-fractures within quartz grains is also common. Cavern-type pores appear frequently, with irregular shapes and sizes varying from 700 to 1700 μm, up to 2900 μm. Sometimes they are interconnected by micro-channels. Caverns are generally larger than in the sample before CO<sub>2</sub> injection. Sometimes, matrix rich bands show elongated channel pores following the anisotropy with a maximum dimension of 4.8 mm. The SEM studies (Fig. 5 b, d and f) showed again intergranular spaces constituted by cavern pores interconnected by micro-channels and pore

**Table 1.** Total porosity of Utrillas sandstones (three samples), before and after SC CO<sub>2</sub>-brine exposure, measured by optical image analysis (OIA). Average % is the average porosity of the three samples.

	Before CO <sub>2</sub> -rich brine		After CO <sub>2</sub> -rich brine		Porosity variation		Interpretation
	Porosity %	Average %*	Porosity %	Average %*	Difference %	Total average %	
Sample 1	18.18		22.05		3.87		
Sample 2	9.55	11.41 ± 0.14	11.13	13.42 ± 0.17	1.58	2.01	increase
Sample 3	6.49		7.06		0.57		

\* Uncertainty (1.25 %) given by Oviedo – IGME Laboratory. Difference % is calculated as the variation in porosity % before and after CO<sub>2</sub>-brine injection. Total average % is the average of the differences between porosity % before and after CO<sub>2</sub>-brine injection.

spaces sometimes filled with minerals. Furthermore, the high degree of fracturing leads to fracture-type pore development.

The pore network quantification by OIA was developed, as previously described, on digital images acquired using objective lens of 10×. The estimated porosity percentage ranges from 7.06 to 22.05 % (Table 1), with an average of 13.42 ± 0.17 %. The maximum area of pore was 250 000 μm<sup>2</sup> and the minimum was 9 μm<sup>2</sup>. The average pore area size was 278 μm<sup>2</sup>. Curves of relative and absolute distribution of number of pores vs. pore area ranges and diagrams of weighted area related to pore area classes are presented in Fig. 6b and d for the samples after SC CO<sub>2</sub> injection.

## 4.2 Chemical analysis

The chemical composition of the brine was analyzed before and after the 24h testing and the results are shown in Table 2. The data of brine composition before and after experimental CO<sub>2</sub> injection show that there were some changes in the chemistry (higher than the total uncertainty of the technique: ≈ 10 %): a decrease (ca. 30 %) of the Ca<sup>2+</sup>, Mg<sup>2+</sup> and SO<sub>4</sub><sup>2-</sup> contents and an increase on the HCO<sub>3</sub><sup>-</sup> and NO<sub>3</sub><sup>-</sup> contents. Other chemical parameters also decreased as a result of the CO<sub>2</sub> injection: the pH changed from 7.2 to 5.27 and the conductivity also decreased around 12 %.

Total rock analyses were performed on blocks with and without experimental CO<sub>2</sub>-brine exposure. The values and uncertainties are presented in Table 3. There were changes in the following contents: increase of MgO (30 %), Na<sub>2</sub>O (20 %) and CaO (ca. 200 %). We considered as significant a change over the uncertainties given by the laboratory for each element, in which uncertainty values range from 6.8 to 19.9 % depending on the element. Two samples were analyzed by XRD, one previous to brine exposure and to SC CO<sub>2</sub> injection and the other after the SC CO<sub>2</sub>-brine experiment. These analyses only detected quartz, the other phases being present in quantities below the detection limit of this technique. Furthermore, the residue that remained in the chamber of the reactor after the experiment was studied (Fig. 7). This residue consisted mainly of quartz in two different fractions:

a fine fraction with sizes around 20 μm and another fraction with rounded quartz grains sometimes reaching 1mm in size.

## 5 Discussion

In the studied Utrillas sandstones, OpM and SEM techniques allowed us to detect qualitative changes in the pore network in the samples before and after SC CO<sub>2</sub> injection. Compared to the pre-experiment samples, we can point out that, in general, after the experiment larger pores are more common (700–1800 μm) and cavern-type pores and channels dominate (Figs. 4a–b and 5a–b). There is also an increase of grain fracturing (Figs. 4c, d and 5c and d). Moreover, the edges of quartz grains before the experiment contain angular pits (Fig. 5e), while pits in quartz after the experiment are less numerous and distinctly rounded and enlarged (Fig. 5f).

Quantification of these changes was systematically carried out applying OIA (Fig. 3). This study reveals an increase of porosity ( $\Delta n$ ) of 0.57–1.58–3.87 % with an average of 2.01 % (Table 1), which value is higher than the uncertainty of the OIA technique (≈ 1.25 %) (Demirmen, 1972; Grove and Jerram, 2011). The lower error of this method as compared to others is one of the advantages of the OIA technique (e.g. error of point counting is around 2.5 %; Chayes and Faibain, 1951; Grove and Jerram, 2011).

The OIA technique also allowed us a complete characterization of the pore network through curves of relative and absolute distribution of the number of pores vs. pore area ranges (Fig. 6) and diagrams of weighted area related to pore area classes for samples before and after SC CO<sub>2</sub> injection. The pore area ranges measured by OIA are between 9 μm<sup>2</sup> and 250000 μm<sup>2</sup>. The distribution of data shows that ≈ 99 % of pores correspond to pores smaller than 1250 μm<sup>2</sup> (Fig. 6a). In the CO<sub>2</sub> injected sample (Fig. 6b) these small pores represent ≈ 98 % of all the pores. The diagrams of the weighted area related to pore area classes before (Fig. 6c) and after SC CO<sub>2</sub> injection (Fig. 6d) show that the contribution of the first class of pore area is ca. 35 % of the total porosity for pre-experiment samples and ca. 25 % of the total porosity for samples after the experiment. The approximate contributions of cumulative weighted pore area for the main percentiles for

**Table 2.** Chemical composition of brine before and after the experiment.

	Brine before CO <sub>2</sub> (mg L <sup>-1</sup> )*	Brine after CO <sub>2</sub> (mg L <sup>-1</sup> )*	Interpretation
Na <sup>+</sup>	2378 ± 237.80	2351 ± 235.10	No change
K <sup>+</sup>	139 ± 13.90	114 ± 11.40	No change
Ca <sup>2+</sup>	570 ± 57.00	440 ± 44.00	Decrease: 30 % ( $\Delta = 130 \text{ mg L}^{-1}$ )
Mg <sup>2+</sup>	268 ± 26.80	200 ± 20.00	Decrease: 34 % ( $\Delta = 68 \text{ mg L}^{-1}$ )
Cl <sup>-</sup>	5200 ± 520	4640 ± 464.00	No change
SO <sub>4</sub> <sup>2-</sup>	624 ± 62.40	464 ± 46.40	Decrease: 34 % ( $\Delta = 160 \text{ mg L}^{-1}$ )
HCO <sub>3</sub> <sup>-</sup>	14 ± 1.40	36 ± 3.60	Increase: 157 % ( $\Delta = 22 \text{ mg L}^{-1}$ )
NO <sub>3</sub> <sup>-</sup>	1.1 ± 0.11	10 ± 0.10	Increase: 809 % ( $\Delta = 8.9 \text{ mg L}^{-1}$ )
SiO <sub>2</sub>	9.3 ± 0.93	8.3 ± 0.83	No change
pH	7.2	5.27	Decrease: 36 % ( $\Delta = 1.93$ )
Conductivity ( $\mu\text{S cm}^{-1}$ )	15 350	13 650	Decrease: 20 % ( $\Delta = 1700 \mu\text{S cm}^{-1}$ )

\* Uncertainty (10%) given by Madrid-IGME Laboratory (Water Analysis).

**Table 3.** Chemical composition of whole rock (Utrillas sandstone) before and after the experiment. Uncertainty given by IGME Laboratory (XRF Analysis).

	Uncertainty (%)	Rock before CO <sub>2</sub> and brine (%)	Rock after CO <sub>2</sub> and brine (%)	Interpretation
SiO <sub>2</sub>	8.20	97.15 ± 2.5260	96.81 ± 2.5430	No change
Al <sub>2</sub> O <sub>3</sub>	11.57	0.98 ± 0.1135	1.12 ± 0.1300	No change
Fe <sub>2</sub> O <sub>3</sub>	9.55	0.30 ± 0.0290	0.28 ± 0.0270	No change
MnO	9.31	0	0	No change
MgO	7.96	0.03 ± 0.0025	0.04 ± 0.0030	Increase: 33 % ( $\Delta = 0.01 \text{ mg L}^{-1}$ )
CaO	6.80	0.04 ± 0.0030	0.12 ± 0.0080	Increase: 200 % ( $\Delta = 0.08 \text{ mg L}^{-1}$ )
Na <sub>2</sub> O	8.20	0.05 ± 0.0040	0.06 ± 0.0050	Increase: 20 % ( $\Delta = 0.01 \text{ mg L}^{-1}$ )
K <sub>2</sub> O	19.94	0.08 ± 0.0160	0.08 ± 0.0160	No change
TiO <sub>2</sub>	8.37	0.03 ± 0.0025	0.03 ± 0.0025	No change
P <sub>2</sub> O <sub>5</sub>	10.95	0.01 ± 0.0010	0.01 ± 0.0010	No change
LOI	12.00	0.48 ± 0.0540	0.64 ± 0.0770	Increase: 33 % ( $\Delta = 0.16 \text{ mg L}^{-1}$ )
TOTAL		99.16	99.20	

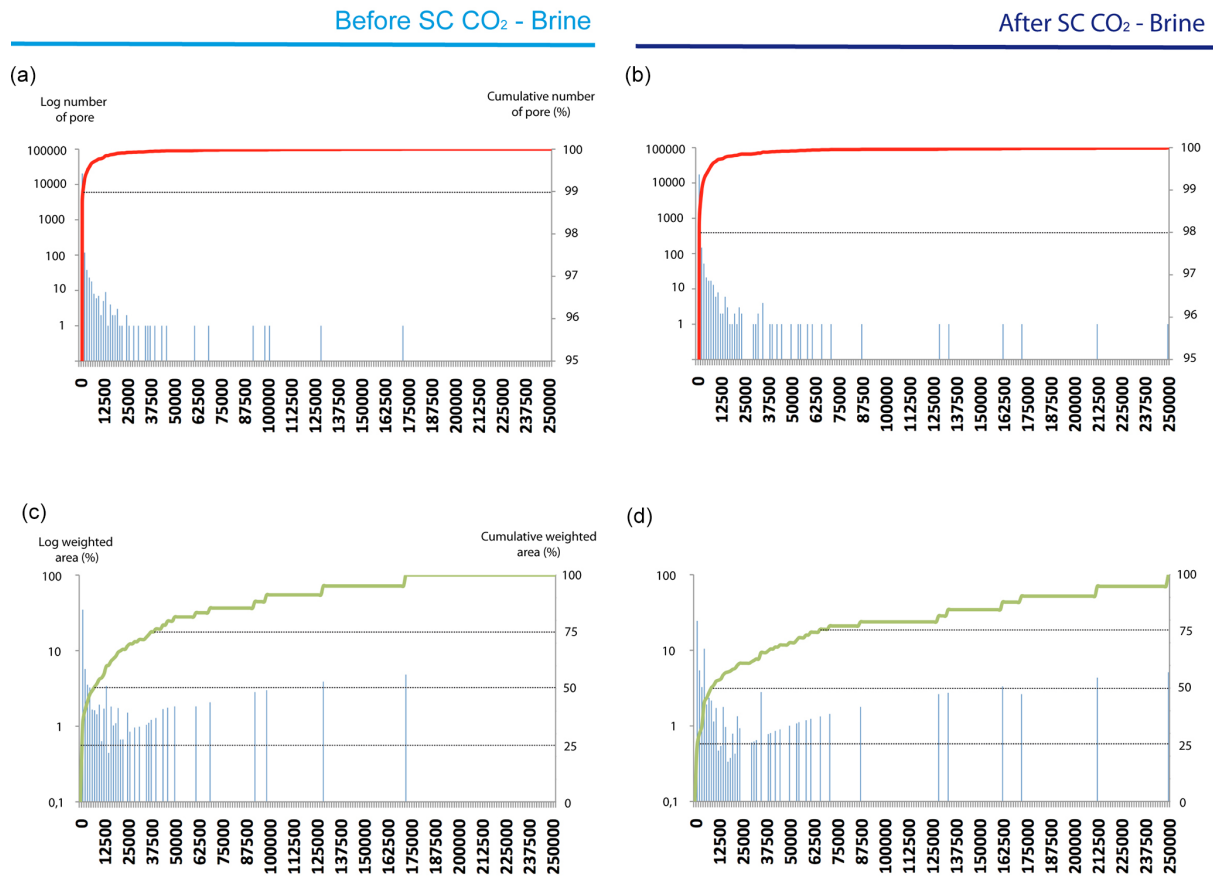
the sample before SC CO<sub>2</sub> injection are the following: < 1250 (25 %), 7500 (50 %) and 38 750  $\mu\text{m}^2$  (75 %). On the other hand, the sample after injection shows contributions of 25 % of pore area of 1250, 50 % of 8750 and 75 % of 65 000  $\mu\text{m}^2$ . In general, in the original samples there are more pores of smaller and intermediate pore area classes than in the ones after the injection. Besides, the maximum sizes of pore area are larger in the injected samples, similarly, Tarkowski and Wdowin (2011) described an increase in the mean pore diameters in their studies.

The brine chemistry study showed that Na<sup>+</sup>, K<sup>+</sup>, Cl<sup>-</sup> and SiO<sub>2</sub> values did not suffer any relevant changes after the injection. On the other hand, the Ca<sup>2+</sup>, Mg<sup>2+</sup> and SO<sub>4</sub><sup>2-</sup> content decreased by approx. 30 % (Table 2), probably all as a result of local mineral precipitation of Mg, Ca and Na min-

erals (e.g. gypsum), evidenced by an increase of these oxides in the chemistry of the rock after the experiment (Table 3).

The brine chemistry data, in relative terms is similar to those found in the literature (Kaszuba et al., 2005), but different to the analysis completed by Tarkowski and Wdowin (2011), Luquot et al. (2012), Yu et al. (2012) and Wdowin et al. (2014a, b). According to them, dissolution of clay and feldspar of the matrix could take place due CO<sub>2</sub>-rich brine. In this case, K<sup>+</sup>, Na<sup>+</sup> and Si<sup>+</sup> could be releases but they do not show relevant variation in the brine analysis after CO<sub>2</sub>.

This is probably due to the initial composition of our samples, conditioned by the chemically resistant quartz (95 % wt.), the short period of our experimentation (24 h) and that interaction between CO<sub>2</sub>-rich brine is limited to external area of the block sandstones studied. We can say that preliminar-

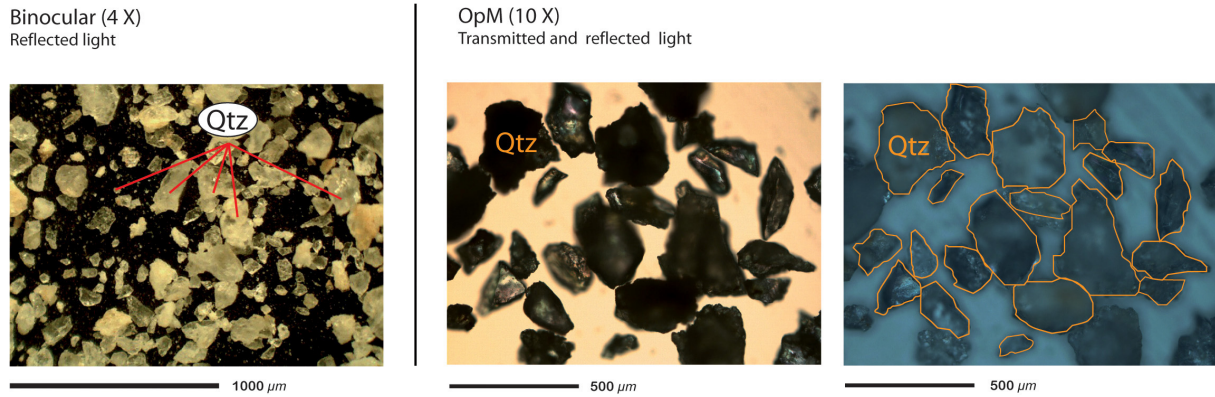


**Figure 6.** (a) X axis vs. left y axis: frequency diagrams of number of pores (Log scale) related to pore area classes ( $\mu\text{m}^2$ ) before CO<sub>2</sub> injection (blue bars). X axis vs. right y axis: cumulative number of pores (%) related to pore area ( $\mu\text{m}^2$ ) (red symbols). Red dashed line represents the contribution of the first class of pore area. (b) X axis vs. left y axis: frequency diagrams of weighted pore area (Log scale) related to pore area ( $\mu\text{m}^2$ ) after CO<sub>2</sub> injection (blue bars). X axis vs. right y axis: cumulative weighted pore area (%) related to pore area classes ( $\mu\text{m}^2$ ) (green symbols). Black dashed lines represent percentiles 25, 50 and 75. (c) X axis vs. left y axis: frequency diagrams of number of pores (Log scale) related to pore area ( $\mu\text{m}^2$ ) before CO<sub>2</sub> injection (blue bars). X axis vs. right y axis: cumulative number of pores (%) related to pore area ( $\mu\text{m}^2$ ) (red symbols). Red dashed line represents the contribution of the first class to pore area. (d) X vs. left y axis: frequency diagrams of weighted pore area (Log scale) related to pore area ( $\mu\text{m}^2$ ) after CO<sub>2</sub> injection (blue bars). X axis vs. right y axis: cumulative weighted pore area (%) related to pore area classes ( $\mu\text{m}^2$ ) (green symbols). Black dashed lines represent percentiles 25, 50 and 75. Minimum pore size considered in the study is  $>9 \mu\text{m}^2$ .

ily CO<sub>2</sub>-brine contact with the rock initiated some mineral precipitation though not to a relevant scale. It also caused brine pH reduction (changing from 7.2 to 5.2), similarly to other cases (Kaszuba et al., 2005; Tarkowski and Wdowin, 2011). The measured pH (5.2) is not representative of the solution pH during the experiment, as it was measured after the experiment during depressurization (Table 2). The pH reduction is due to the increase of carbonic acid and NO<sub>3</sub><sup>-</sup> content of the brine after the experiment. The higher amount of carbonic acid originates from the CO<sub>2</sub> dissolution in the brine, and could allow carbonation and formation of CaCO<sub>3</sub> and MgCO<sub>3</sub> due to the depressurization process followed, while that of the NO<sub>3</sub><sup>-</sup> may be due to reactions with organic material present in the rock sample. The overall data of the total rock composition of before and after SC CO<sub>2</sub>-brine exposure

do not show important precipitation/dissolution of mineral phases. We can conclude that the reactions between minerals and fluids were not significant (Gunter et al., 1997; Hitchon, 1996), and the changes in the porosity configuration measured (Table 1) are limited to external areas of the sandstone blocks exposed to CO<sub>2</sub>-rich brine and probably due to local chemical changes; and may represent the early physical display of the chemical influence of the CO<sub>2</sub>-rich brine on the rock.

The observed and measured changes in the studied samples are due to the CO<sub>2</sub>-rich brine exposure and can be of importance in the vicinity of the injection well (Fig. 1a) where the interaction of the CO<sub>2</sub> and the rock takes place initially in wet conditions (Kharaka et al. 2006; Gaus, 2010; André et al., 2007). Any modification in mineralogy and porosity

Qtz: after SC CO<sub>2</sub> - Brine

**Figure 7.** Photomicrographs by binocular microscope (reflected light) and by optical microscope (transmitted and reflected light) of the residue that remained in the reactor chamber after the experiment.

(Figs. 4, 5 and Table 1) changing the rock texture could affect the injection well and its closest environment and hence the injection efficiency (Wdowin et al., 2014a). Our experimental investigation indicates that the main effects observed after the experiment are relevant to the pore network characteristics and quantification, while changes regarding chemical characteristics of the brine and total rock are minor. The initial heterogeneity of the rock could condition the comparison of physical and chemical parameters between the before and after CO<sub>2</sub> injection tests samples, as described by Tarkowski and Wdowin (2011) and Wdowin et al. (2014b). In our study we tried to minimize this effect studying rock surfaces few millimetres separation and employing expert criteria in petrography.

The porosity changes observed could be understood by the following simplified conceptual model (Fig. 8a to d). The CO<sub>2</sub>-rich brine interaction with saturated samples produces a change in the external surface of the sandstone blocks. These effects resulted in a partial loss of the quartz (both skeletal grains and matrix), present as residue after the experiment (Fig. 7). Our conceptual model consists of four stages.

- Stage 1 (Fig. 8a): Initial mineralogical and textural conditions of the rock saturated with brine. Quartz constitutes 95 % of the rock sample and brine filling intergranular spaces.
- Stage 2 (Fig. 8b): pressurized SC CO<sub>2</sub> injection: initial CO<sub>2</sub> input would enrich the brine with CO<sub>2</sub> (at sub-critical CO<sub>2</sub> conditions), in which the samples are immersed. This CO<sub>2</sub>-rich brine will interact with the rock and the brine that is inside the pore network. We assume that the acidified brine interacts with the brine that is filling the pores. The low compressibility coefficient of a fluid in the case of an increase of pressure and temperature (as in this experiment) does not favour displacements of the fluid.

- Stage 3 (Fig. 8c): pressurized CO<sub>2</sub> / CO<sub>2</sub>-rich brine stabilization: this stage extends through most of the experimental run (24 h). During this time, CO<sub>2</sub>-rich brine continues interacting with the rock and brine in the pores under SC CO<sub>2</sub> conditions.
- Stage 4 (Fig. 8d): CO<sub>2</sub> / CO<sub>2</sub>-rich brine pressure and temperature decrease to ambient conditions: CO<sub>2</sub>-rich brine will continue to interact with the rock until ambient conditions are reached.

During this phase there is a leak of quartz particles and matrix that were collected in the chamber when the experiment was finished. Furthermore, internal quartz breakdown and generation of free micro-quartz grains (Figs. 4b, d and f; 5b, d and f) were observed by OpM.

This model (at thin section scale of surface block rocks), explains how the changes identified by OpM, SEM Figs. 4 and 5, probably were originated by the chemical influence of the CO<sub>2</sub>-rich brine on the saturated rocks. In particular the action of CO<sub>2</sub>-rich brine could produce a de-cohesion/dissolution of the matrix, leading an increase in the porosity. The chemical analyses (0.27 dm<sup>3</sup> rock blocks and 0.3 dm<sup>3</sup> brines) did not show major dissolution/precipitation processes at these early stages, probably also due to an effect of the scale of analysis.

## 6 Conclusions

Quantitative assessment of petrography and mineralogy by OIA can be an important tool for geosciences, providing numerical values as a key to the successful interpretation of the rock texture and mineralogy.

The proposed methodology, consisting of mineralogical and petrographic studies by OpM, SEM and OIA techniques on sandstones subjected to CO<sub>2</sub>-rich brine exposure

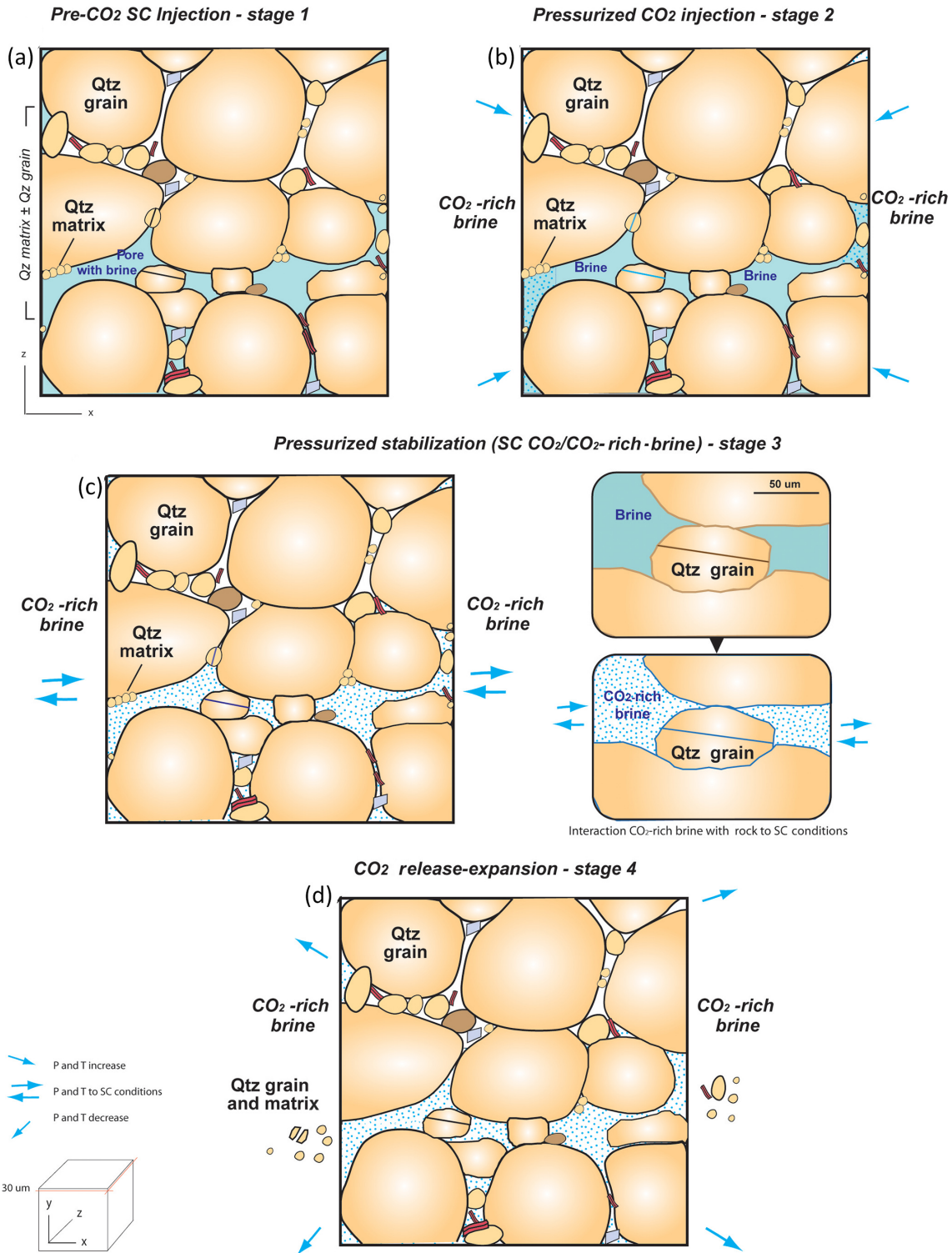


**Figure 8.** Scheme of a simplified model developed from the observed mineralogical/textural changes after the SC CO<sub>2</sub> injection in the Utrillas sandstones. As a summary, (a) initial mineralogy and texture of the sandstones: quartz is the 95 % of the rock sample and brine filling intergranular spaces. (b) When the pressurized SC CO<sub>2</sub> injection begins, the injected gas acidified the brine (CO<sub>2</sub>-rich brine) and it interacts with the rock and the brine that is inside the pore network. (c) During supercritical experimental stage, the pressurized CO<sub>2</sub>-rich brine and brine interact under SC conditions producing instability in the original rock cohesion probably due to local chemical changes. (d) Released pressure at the end stage of the experiment may produce the leaks of quartz particles and matrix.

(7.8 MPa, 38 °C, during 24 h), proved to be highly effective for the identification and measurement of changes in the pore network. For this study, the Utrillas sandstones were selected due to their potential as CO<sub>2</sub> reservoir in Spain. However, the same methodology could be applicable for future studies considering other rock types, different CO<sub>2</sub> storage conditions or longer periods of exposure time.

The influence of the original rock composition and texture is very important and leads to different effects of the CO<sub>2</sub>-rich brine exposure. The study of potential changes at the rock matrix scale depends on the facies variations of any sedimentary formation, when evaluating a possible CO<sub>2</sub> reservoir. The facies studied in this work is characterized by 95 % quartz content and heterogeneous rock texture, where micro-channels in the quartz matrix areas favour the SC CO<sub>2</sub>-brine injection resulting in the development of bigger cavities and pore channels. The main pore evolution measured by OIA was an increase of porosity (2.01 %) and a readjustment of pore-network distribution regarding pore size classes.

The chemical-compositional evolution of the analyzed elements did not evidence significant mineralogical processes. Supercritical CO<sub>2</sub> causes brine pH to decrease as a consequence of carbonic acid increase. Some improvements would allow understand the chemical processes occurring in the experiments: e.g. number of analyses, elements to analyze, accuracy of techniques and use of PHREEQC models.

The results of this experiment show that the changes occurred due to chemical interaction of the acidified brine allowing a rough approximation of the CO<sub>2</sub>-brine-rock interactions. Furthermore, these changes may have an important impact on the behaviour of reservoir rocks during first injection phases of SC CO<sub>2</sub>: (i) changes in the rock system that lead to the porosity evolution could facilitate further CO<sub>2</sub> injection; (ii) mobilization of solid material (quartz) should be considered during experiments and/or future modelling of the reservoir.

*Acknowledgements.* The authors would like to thank the funding provided through the ALGECO2-IRMC Project (Instituto Geológico y Minero de España: 2294-2013), CO<sub>2</sub>-Pore Project (Plan Nacional de España: 2009-10934, FEDER-UE), Minería XXI Project (CYTED: 310RT0402) and DIA-CO<sub>2</sub> Projects I and II (CIUDEN: ALM/09/032 and ALM/12/028). Thanks are due to Roberto Martínez, Félix Mateos, Luís González-Menéndez, Isabel Suárez and Ricardo Molinero for providing help in OIA techniques, SEM analysis, data acquisition and statistical treatment for rock sample collection and to Timea Kovacs for her suggestions. We also would like to thank J. Alvarez-Marron for the editorial handling and two anonymous reviewers for their constructive comments and corrections.

Edited by: J. Alvarez-Marron

## References

- Alonso, J. L., Pulgar, J. A., García-Ramos, J. C., and Barba, P.: Tertiary basins and Alpine tectonics in the Cantabrian Mountains (NW Spain), in: Tertiary basins of Spain: The stratigraphic record of crustal Kinematics, edited by: Friend, P. F. and Dabrio, C. J., Cambridge University Press, Cambridge, 214–227, 1996.
- André, L., Audigane, P., Azaroual, M., and Menjot, A.: Numerical modelling of fluid-rock chemical interactions at the supercritical CO<sub>2</sub>-liquid interface during CO<sub>2</sub> injection into a carbonate reservoir, the Dogger aquifer (Paris Basin, France), *Energ. Convers. Manage.*, 48, 1782–1797, 2007.
- Bacci, G., Korre, A., and Durucan, S.: An experimental and numerical investigation into the impact of dissolution/precipitation mechanisms on CO<sub>2</sub> injectivity in the wellbore and far field regions, *Int. J. Greenh. Gas Con.*, 5, 579–588, 2011.
- Bachu, S.: Sequestration of CO<sub>2</sub> in geological media: criteria and approach for site selection in response to climate change, *Energ. Convers. Manage.*, 41, 953–970, 2000.
- Benson, S. M. and Cole, D. R.: CO<sub>2</sub> sequestration in deep sedimentary formations, *Elements*, 4, 325–331, 2008.
- Berrezueta, E., González-Menéndez, L., Breitner, D., and Luquot, L.: Pore system changes during experimental CO<sub>2</sub> injection into detrital rocks: Studies of potential storage rocks from some sedimentary basins of Spain, *Int. J. Greenh. Gas Con.*, 17, 411–422, 2013.
- Berrezueta, E., González-Menéndez, L., Ordoñez-Casado, B., and Olaya, P.: Pore network quantification of sandstones under experimental CO<sub>2</sub> injection using Image Analysis, *Comput. Geosci.*, 77, 97–110, 2015.
- Bertier, P., Swennen, R., Laenen, B., Lagrou, D., and Dreesen, R.: Experimental identification of CO<sub>2</sub>-water-rock interactions caused by sequestration of CO<sub>2</sub> in Westphalian and Buntsandstein sandstones of the Campine Basin (NE-Belgium), *J. Geochem. Explor.*, 89, 10–14, 2006.
- Burton, M., Kumar, K., and Bryant, S. L.: Time-dependent injectivity during CO<sub>2</sub> storage in aquifers, in: Symposium on Improved Oil Recovery Tulsa, Okla, Proceedings: Richardson, Tex., Society of Petroleum Engineers, paper SPE 113937, p. 15, 2008.
- Cailly, B., Le Thiez, P., Egermann, P., Audibert, A., Vidal-Gilbert, S., and Longaygue, X.: Geological storage of CO<sub>2</sub>: A state-of-the-art of injection processes and technologies, *Oil Gas Sci. Technol.*, 60, 517–525, 2005.
- Chayes, F. and Fairbairn, H. W.: A test of the precision of thin-section analysis by point counter, *Am. Mineral.*, 36, 704–712, 1951.
- Choquette, P. W. and Pray, L. C.: Geologic nomenclature and classification of porosity in sedimentary carbonates, *AAPG bulletin*, 54, 207–250, 1970.
- Demirmen, F.: Operator error in petrographic point-count analysis: a theoretical approach, *J. Int. Assoc. Mathemat. Geol.*, 4, 35–43, 1972.
- Desbois, G., Urai, J. L., Kukla, P. A., Konstanty, J., and Baerle, C.: High-resolution 3D fabric and porosity model in a tight gas sandstone reservoir: a new approach to investigate microstructures from mm-to nm-scale combining argon beam cross-sectioning and SEM imaging, *J. Petrol. Sci. Engin.*, 78, 243–257, 2011.
- Egermann, P., Bazin, B., and Vizika, O.: An experimental investigation of reaction-transport phenomena during CO<sub>2</sub> injection, in:

- SPE Middle East Oil Show, Bahrain, Soc. Petrol. Engin. Paper 93674, 2005.
- Evers, H. J.: Geology of the Leonies between the Bernesga and Porma rivers, Cantabrian Mountains, NW Spain, *Leidse Geologische Mededelingen*, 41, 83–151, 1967.
- Fischer, S., Liebscher, A., De Lucia, M., and Hecht, L.: Reactivity of sandstone and siltstone samples from the Ketzin pilot CO<sub>2</sub> storage site-Laboratory experiments and reactive geochemical modelling, *Environ. Earth Sci.*, 70, 3687–3708, 2013.
- Folk, R. L.: *Petrology of Sedimentary Rocks*, Hemphill's, Austin, Texas, 170 pp., 1974.
- Gallastegui, J.: Estructura cortical de la Cordillera y Margen Continental Cantábricos: Perfiles ESCI-N, Trabajos de Geología, Universidad de Oviedo, 22, 9–234, 2000.
- García Lobón, J. L., Reguera García, M. I., Martín León, J., Rey Moral, C., and Berrezueta, E.: Plan de selección y caracterización de áreas y estructuras favorables para el almacenamiento geológico de CO<sub>2</sub> en España, Resumen ejecutivo Instituto Geológico y Minero de España (IGME), Madrid, 2010.
- Gaus, I.: Role and impact of CO<sub>2</sub>-rock interactions during CO<sub>2</sub> storage in sedimentary rocks, *Int. J. Greenh. Gas Con.*, 4, 73–89, 2010.
- Gaus, I., Audigane, P., Andre, L., Lions, J., Jacquement, N., Durst, P., Czernichowski, I., and Azaroual, M.: Geochemical and solute transport modelling for CO<sub>2</sub> storage, what to expect from it?, *Int. J. Greenh. Gas Con.*, 2, 605–625, 2008.
- Grove, C. and Jerram, D. A.: jPOR: An ImageJ macro to quantify total optical porosity from blue-stained thin sections, *Comput. Geosci.*, 37, 1850–1859, 2011.
- Gunter, W. D., Wiwehar, B., and Perkins, E. H.: Aquifer disposal of CO<sub>2</sub>-rich greenhouse gases: extension of the time scale of experiment for CO<sub>2</sub>-sequestering reactions by geochemical modelling, *Mineral. Petrol.*, 59, 121–140, 1997.
- Gunter, W. D., Bachu, S., and Benson, S.: The role of hydrogeological and geochemical trapping in sedimentary basins for secure geological storage of carbon dioxide, *Geological Society, London, Special Publications*, 233, 129–145, 2004.
- Hitchon, B.: Aquifer disposal of carbon dioxide: hydrodynamic and mineral trapping-proof of concept, Geoscience Publishing Ltd, Alberta, Canada, 165 pp., 1996.
- Holloway, S.: An overview of the underground disposal of carbon dioxide, *Energ. Convers. Manage.*, 38, S193–S198, 1997.
- Izgec, O., Demiral, B., Bertin, H. J., and Akin, S.: Experimental and numerical investigation of carbon sequestration in saline aquifers, in: SPE/EPA/DOE Exploration and Production Environmental Conference, Galveston, Texas, Soc. Petrol. Engin. Paper 94697, 2005.
- Izgec, O., Demiral, B., Bertin, H. J., and Akin, S.: CO<sub>2</sub> injection into saline carbonate aquifer formations I: laboratory investigation, *Transport in Porous Media*, 72, 1–24, 2008.
- Kaszuba, J. P., Janecky, D. R., and Snow, M. G.: Carbon dioxide reaction processes in a model brine aquifer at 200 °C and 200 bars: implications for geologic sequestration of carbon, *Appl. Geochem.*, 18, 1065–1080, 2003.
- Kaszuba, J. P., Janecky, D. R., and Snow, M. G.: Experimental evaluation of mixed fluid reactions between supercritical carbon dioxide and NaCl brine: Relevance to the integrity of a geologic carbon repository, *Chem. Geol.*, 217, 277–293, 2005.
- Ketzer, J. M., Iglesias, R., Einloft, S., Dullius, J., Ligabue, R., and De Lima, V.: Water-rock-CO<sub>2</sub> interactions in saline aquifers aimed for carbon dioxide storage: experimental and numerical modeling studies of the Rio Bonito Formation (Permian), southern Brazil, *Appl. Geochem.*, 24, 760–767, 2009.
- Kharaka, Y. K., Cole, D. R., Hovorka, S. D., Gunter, W. D., Knauss, K. G., and Freifeld, B. M.: Gas-water-rock interactions in Frio Formation following CO<sub>2</sub> injection: Implications for the storage of greenhouse gases in sedimentary basins, *Geology*, 34, 577–580, 2006.
- Lake, L. W.: *Enhanced oil recovery*, Pentice Hall, Englewood Cliffs, NJ, 1989.
- Liu, H., Hou, M.Z., Gou, Y., and Were, P.: Simulation of CO<sub>2</sub>-Water-Rock Interaction Processes-Mineral Scaling Problems in Saline Formations, in: Clean energy systems in the subsurface: production, storage and conversion, Springer Series in Geomechanics and Geoengineering, 233–248, 2013.
- Lobato, L., García-Alcalde, J. L., Sánchez de Posada, L. C., Truyols, J., and Servicio Geológico, S. A. H. V. L. (Cuenca Cñera-Matallana): Mapa geológico de España a E, 1 : 50.000, núm. 104 “Boñar”, Segunda Serie, Primera Edición, Instituto Geológico y Minero de España (IGME), Madrid, 1985.
- Lucia, F. J.: *Carbonate reservoir characterization*: Berlin, Springer-Verlag, 226 pp., 1999.
- Luquot, L. and Gouze, P.: Experimental determination of porosity and permeability changes induced by injection of CO<sub>2</sub> into carbonate rocks, *Chem. Geol.*, 265, 148–159, 2009.
- Luquot, L., Andreani, M., Gouze, P., and Camps, P.: CO<sub>2</sub> percolation experiment through chlorite/zeolite-rich sandstone (Pretty Hill Formation-Otway Basin-Australia), *Chem. Geol.*, 294, 75–88, 2012.
- Manjón Rubio, M., Vargas Alonso, I., Colmenero Navarro, J. R., García-Ramos, J. C., Gutiérrez Elorza, M., and Molina, E.: Memoria del Mapa geológico de España E. 1 : 50.000, Hoja núm. 130 (Vegas del Condado), Segunda Serie, Primera Edición, Instituto Geológico y Minero de España (IGME), Madrid, 1982a.
- Manjón Rubio, M., Vargas Alonso, I., Colmenero Navarro, J. R., García-Ramos, J. C., Crespo Zamorano, A., and Matas González, J.: Mapa geológico de España E, 1 : 50.000, Hoja núm. 130 (Vegas del Condado), Segunda Serie, Primera Edición, Instituto Geológico y Minero de España (IGME), Madrid, 1982b.
- Martínez, R., Suarez, I., Carneiro, J., Zarhlou, Y., Le Nindre, Y., and Boavida, D.: Storage capacity evaluation for development of CO<sub>2</sub> infrastructure in the west Mediterranean, *Energy Procedia*, 37, 5209–5219, 2013.
- Mito, S., Xue, Z., and Ohsumi, T.: Case study of geochemical reactions at the Nagaoka CO<sub>2</sub> injection site, Japan, *Int. J. Greenh. Gas Con.*, 2, 309–318, 2008.
- Olivé Davó, A., Álvaro López, M., Ramírez del Pozo, J., and Aguilar Tomás, M.: Memoria del Mapa Geológico de España a Escala 1 : 200.000, Hojas N° 5/12 (Bermeo/Bilbao), Instituto Tecnológico Geominero de España, Madrid, 208 pp., 1989.
- Perkins, E. H. and Gunter, W. D.: Aquifer disposal of CO<sub>2</sub>-rich greenhouse gasses: modelling of water-rock reaction paths in a siliciclastic aquifer, in: *Water-rock Interactions*, edited by: Kharaka, Y. K. and Chidaev, O. V., Brookfield, Rotterdam, 895–898, 1995.
- Pettijohn, F. J., Potter, P. E., and Siever, R.: *Sand and Sandstones*, Springer, Berlin, 553 pp., 1987.

- Quintana, L., Pulgar, J. A., and Alonso, J. L.: Displacement transfer from borders to interior of a plate: a crustal transect of Iberia, *Tectonophysics*, 663, 378–398, 2015.
- Rochelle, C. A., Czernichowski-Lauriol, I., and Milodowski, A. E.: The impact of chemical reactions on CO<sub>2</sub> storage in geological formations: a brief review, Geological Society, London, Special Publications, 233, 87–106, 2004.
- Rosenbauer, R. J., Koksalan, T., and Palandri, J. L.: Experimental investigation of CO<sub>2</sub>-brine-rock interactions at elevated temperature and pressure: implications for CO<sub>2</sub> sequestration in deep-saline aquifers, *Fuel Proc. Technol.*, 86, 1581–1597, 2005.
- Ross, G. D., Todd, A. C., Tweedie, J. A., and Will, A. G.: The Dissolution Effects of CO<sub>2</sub>-Brine Systems on the Permeability of UK and North Sea Calcareous Sandstones. In SPE/DOE 10685 Enhanced Oil Recovery Symposium, Society of Petroleum Engineers, 1982.
- Rupke, J.: The Esla Nappe, Cantabrian Mountains (Spain), *Leidsche Geologische Mededelingen*, 32, 1–74, Leiden, 1965.
- Saeedi, A., Rezaee, R., Evans, B., and Clennell, B.: Multiphase flow behaviour during CO<sub>2</sub> geo-sequestration: Emphasis on the effect of cyclic CO<sub>2</sub>-brine flooding, *J. Petrol. Sci. Engin.*, 79, 65–85, 2011.
- Sayegh, S. G., Krause, F. F., Girard, M., and DeBree, C.: Rock/fluid interactions of carbonated brines in a sandstone reservoir: Pembina Cardium, Alberta, Canada, *SPE Formation Evaluation*, 5, 399–405, 1990.
- Span, R. and Wagner, W.: A new equation of state for carbon dioxide covering the fluid region from the triple-point temperature to 1100 K at pressures up to 800 MPa, *J. Phys. Chem. Referen. Data*, 25, 1509–1596, 1996.
- Sterpenich, J., Sausse, J., Pironon, J., Géhin, A., Hubert, G., Perfetti, E., and Grgic, D.: Experimental ageing of oolitic limestones under CO<sub>2</sub> storage conditions: Petrographical and chemical evidence, *Chem. Geol.*, 265, 99–112, 2009.
- Svec, R. K. and Grigg, R. B.: Physical effects of WAG fluids on carbonate core plugs. In SPE 71496 Annual Technical Conference and Exhibition, Society of Petroleum Engineers, 2001.
- Tarkowski, R. and Wdowin, M.: Petrophysical and mineralogical research on the influence of CO<sub>2</sub> injection on Mesozoic reservoir and caprocks from the polish lowlands, *Oil Gas Sci. Technol.–Revue d’IFP Energies Nouvell.*, 66, 137–150, 2011.
- Tarkowski, R., Wdowin, M., and Manecki, M.: Petrophysical examination of CO<sub>2</sub>-brine-rock interactions-results of the first stage of long-term experiments in the potential Zaosie Anticline reservoir (central Poland) for CO<sub>2</sub> storage, *Environ. Monit. Assess.*, 187, 1–10, 2015.
- Vickerd, M. A., Thring, R. W., Arocena, J. M., Li, J. B., and Heck, R. J.: Changes in porosity due to acid gas injection as determined by X-ray computed tomography, *J. Can. Petrol. Technol.*, 45, 6 pp., 2006.
- Wdowin, M., Tarkowski, R., and Franus, W.: Determination of changes in the reservoir and cap rocks of the Chabowo Anticline caused by CO<sub>2</sub>-brine-rock interactions, *Int. J. Coal Geol.*, 130, 79–88, 2014a.
- Wdowin, M., Tarkowski, R., and Franus, W.: Supplementary Studies of Textural and Mineralogical Changes in Reservoir and Caprocks from Selected Potential Sites Suitable for Underground CO<sub>2</sub> Storage, *Arab. J. Sci. Engin.*, 39, 295–309, 2014b.
- Yu, Z., Liu, L., Yang, S., Li, S., and Yang, Y.: An experimental study of CO<sub>2</sub>-brine-rock interaction at in situ pressure-temperature reservoir conditions, *Chem. Geol.*, 326/327, 88–101, 2012.